Computers and Concrete, *Vol. 20, No. 3 (2017) 297-310*
DOI: https://doi.org/10.12989/cac.2017.20.3.297

Numerical simulation of dynamic segregation of self-consolidating concrete (SCC) in T-box set-up

Masoud Hosseinpoor[*1], Kamal H. Khayat[2a] and Ammar Yahia[1b]

[1]*Department of Civil Engineering, Université de Sherbrooke, 2500 boul. de l'Université, Sherbrooke, Québec, Canada*
[2]*Department of Civil, Architectural and Environmental Engineering, Missouri University of Science and Technology, 224 Engineering Research Lab, Rolla, MO, USA*

(Received October 1, 2016, Revised March 25, 2017, Accepted April 28, 2017)

Abstract. A CFD software was used to simulate free surface flow of SCC in the T-Box test. In total, seven simulations were developed to study the effect of rheological parameters on the non-restricted flow performance of SCC in both horizontal and vertical directions. Different suspending fluids having five plastic viscosity values between 10 and 50 Pa.s, three yield stress values between 14 and 75 Pa, one density of 2500 kg/m^3, and one shear elasticity modulus of 100 Pa were considered for suspension of 178 spherical particles of 20-mm diameter and 2500 kg/m^3 density. The results of the simulations are found to correlate well to changes in rheological parameters of the suspending fluid. Plastic viscosity was shown to be the most dominant parameter affecting flowability and dynamic stability compared to the yield stress. A new approach was proposed to evaluate performability of SCC based on a trade-off between flowability and dynamic stability.

Keywords: dynamic stability; flowability; performability; self-consolidating concrete; T-Box test

1. Introduction

Self-consolidating concrete (SCC) is a novel construction material that is gaining market acceptance in various applications. Higher fluidity characteristics of SCC enable it to be used in some special applications, such as densely reinforced sections. However, higher flowability of SCC makes it more sensitive to segregation of coarse particles during flow (i.e., dynamic segregation) and thereafter at rest (i.e., static segregation) (ACI 237R-07, Assaad *et al*. 2004, Khayat *et al*. 2004).

Dynamic segregation corresponds to the separation of coarse aggregates from the mortar matrix during flow (Thrane 2007). It can result in less aggregate content in top layers of the cast concrete, which is called vertical dynamic segregation. This type of segregation is more important in the case of vertical applications, such as tremie concreting and casting of tall wall and column elements. This can be accelerated by gravitational induced and static segregation (Leighton and Arcrivos 1987, Zhaosheng *et al*. 2007, Gunes *et al*. 2008, Spangenberg *et al*. 2012a and 2012b, Liao *et al*. 2016). On the other hand, increasing horizontal flow distance can result in less coarse aggregate content at flow front, regardless of the effect of the obstacles and blocking resistance. This is called horizontal dynamic segregation which is more concerned in horizontal applications, such as casting of long slabs, beams, and wall elements (Khayat and Mitchell 2009). Therefore, comparison between the properties of SCC at each horizontal or vertical levels and the casting point, i.e., the point where the concrete is dropped into the formwork, can lead to evaluate the dynamic stability of the mixtures on that level.

Accordingly, new experimental tests are developed, including determination of coarse particle contents in different horizontal and vertical sections of a channel (Shen *et al*. 2009 and 2015a) and penetration depth which measures the depth of the thickness of the cement mortar/paste accumulated above the settled aggregates (ASTM C1712-14 and Shen *et al*. 2014). For example, SCC is allowed to flow in a channel and then the particle content at the entrance and the end of the channel are compared to determine the horizontal dynamic segregation (Shen *et al*. 2015b). Turgut *et al*. (2012) developed a modified L-Box set-up to evaluate the dynamic segregation of SCC in different locations in the horizontal channel. Sonebi *et al*. (2007) proposed a settlement column segregation test which comprises a small column of SCC being subjected to a controlled jolting action followed by 5 minutes settlement period. Accordingly, the segregation obtained by this set-up is a combination of both dynamic and static segregation, corresponding to the jolting action and the settlement period, respectively.

The T-Box test which resembles the non-restricted flow of the SCC by tilting motion of the box in different rotating cycles was developed (Esmaeilkhanian 2011, Esmaeilkhanian *et al*. 2014a). Displacement of the mass-center of the concrete during rotation process can simulate the motion of concrete in the formwork in vertical and horizontal directions. Vertical and horizontal dynamic segregation of SCC are then measured by determining the penetration depths and coarse aggregate contents at two

∗Corresponding author, Postdoctoral Fellow
E-mail: masoud.hosseinpoor@usherbrooke.ca
[a]Professor
[b]Associate Professor

http://www.techno-press.org/?journal=cac&subpage=8 ISSN: 1598-8198 (Print), 1598-818X (Online)

sides of the box, respectively. Esmaeilkhanian *et al*. (2014b) evaluated experimentally the effect of mix design parameters and rheological properties of SCC on the results obtained by T-Box test. It was revealed that increasing yield stress and plastic viscosity can result in higher dynamic stability of SCC due to higher drag force exerted by the mortar matrix on coarse aggregates. Consequently, workability parameters of SCC have a significant effect on its dynamic stability. For example, decreasing slump flow from 700 to 640 mm and increasing V-Funnel flow time from 5 to 25 s could result in increasing the dynamic stability of SCC up to 38% to 50%. This is due to higher plastic viscosity and yield stress of the mixture (Esmaeilkhanian 2011, Esmaeilkhanian *et al*. 2014a and 2014b). It was also concluded that ensuring proper dynamic segregation resistance is more stringent than static segregation (Esmaeilkhanian *et al*. 2014b).

Disturbing the homogeneity of fresh SCC mixtures results in negative effects on its structural performance and durability in the hardened state. Therefore, there is a great need to develop some theoretical tools to evaluate stability of SCC during the casting process. Using these tools can lead to assess the required conditions to ensure proper dynamic stability and flowability. It must be noted that there is always a trade-off between dynamic stability and flowability of SCC that should be established given the casting conditions (Khayat 1999). Numerical simulations of flow of SCC can be considered as powerful tool to predict flow performance of the mixture while taking into account flow induced segregation (Roussel *et al*. 2007 and 2016, Yammine *et al*. 2008). Recently, there is a great interest to employ computational flow modeling to evaluate the dynamic stability of SCC (Thrane 2007, Spangenberg *et al*. 2012a and 2012b, Roussel *et al*. 2016). Spangenberg *et al*. (2012a and 2012b) studied different patterns of dynamic segregation of SCC. The results showed that gravitational particle segregation plays the dominant role in dynamic segregation of the coarsest aggregates in both horizontal and vertical directions during the casting process.

In this paper, a computational fluid dynamics (CFD) software was employed to simulate free surface flow of SCC in the T-Box test apparatus as a heterogeneous suspension of coarse particles in a Bingham surrounding fluid. The Navier–Stokes and conservation of mass equations for incompressible materials are solved by the volume of fluid (VOF) method (Hirt and Nichols 1981). In total, 7 simulations were developed to study the effect of rheological parameters of the suspending fluid on flowability and non-restricted dynamic stability of SCC in both horizontal and vertical directions. Modelled suspensions consisted of the suspending fluid that corresponds to the stable homogeneous portions of the SCC mixture, which includes the fraction of the coarse and fine aggregates that can flow in a homogeneous manner during the casting process. Several suspending fluids with various yield stress and plastic viscosity values were investigated. The paper discusses the results of the numerical simulations in terms of flow velocity, strain rate, kinetic energy, flow profiles, and particle distribution throughout the T-Box channel (horizontal direction) and fluid depth (vertical direction) following six tilting cycles of the T-Box test.

2. T-Box test set-up

The T-Box test set-up was developed to evaluate dynamic stability of SCC (Esmaeilkhanian 2011, Esmaeilkhanian *et al*. 2014a and 2014b). As can be observed in Fig. 1, the proposed apparatus consists of a rectangular channel measuring 1 m in long, 0.2 m in width, and 0.4 m in height, hinged in the middle to a 140-mm height support. The rotating motion of the box is limited by another support beneath one end of the channel. An amount of 16 L of SCC is cast in the channel which provides an initial concrete thickness of 80 mm (Esmaeilkhanian 2011). This test simulates the flow distance traveled by the concrete (typically SCC) in the formwork using a tilting motion of the box in given rotating cycles. Each single 2-s flow cycle is reached when the channel rotates from the initial horizontal position in the non-supported side till the box touches the floor in 1-s half cycle (i.e., titling down), and then moves back to the horizontal state in another 1 s (i.e., tilting up) in a continuous motion. Consequently, as the number of cycle increases, the coarse particles accumulate gradually in the tilt down section, and at the same time this results in formation of a layer of mortar in the top surface of the concrete placed in the tilt up section. Comparing the properties of the concrete in the tilt down section to the one placed in the tilt up section in a given number of tilting cycles can enable the evaluation of dynamic stability of the investigated mixture. In this paper, flow performance of various SCC mixtures are evaluated in T-Box set-up using CFD.

3. Properties of modelled materials and T-Box test procedure

The investigated SCC mixtures are considered as suspensions of coarse particles in various suspending fluids. The suspending fluid is assumed actually as the portion of the concrete mixture that shows no segregation and keeps homogeneous during flow. The parameters of the modeling included five plastic viscosity values (10, 17, 25, 38, and 50 Pa.s), three yield stress values (14, 45, and 75 Pa), and a density of 2500 kg/m^3, as well as one shear elasticity modulus value of 100 Pa for the suspending fluids. The shear elasticity modulus is the ratio of the shear stress to shear strain in the elastic state of the suspending fluid. Selected values of rheological parameters (i.e., plastic viscosity of 10 to 50 Pa.s, and yield stress of 14 to 75 Pa) correspond to rheological parameters of suspending fluids that can ensure flowable SCC having risk of dynamic segregation. This can allow the evaluation of the effect of rheological parameters of the suspending fluid on dynamic stability of SCC mixtures.

The virtual concrete suspensions included 178 spherical particles of 20-mm diameter which corresponds to 4.7% volumetric particle content. Indeed, it was assumed that the finer coarse aggregate fraction that can remain in homogeneous suspension in the SCC mixture during the flow period makes up part of the suspending fluid. Accordingly, the suspending fluid can be assumed as the stable portion of the SCC mixture. It can be explained by

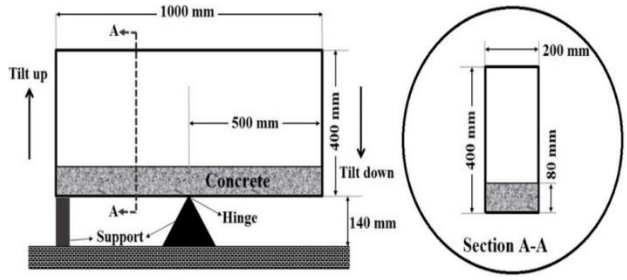

Fig. 1 Schematics of T-Box set-up (Esmaeilkhanian 2011, Esmaeilkhanian *et al.* 2014a, 2014b)

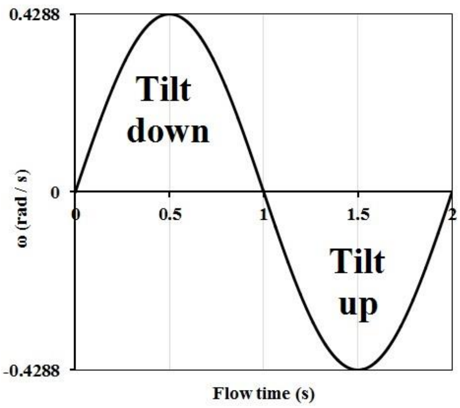

Fig. 2 Angular velocity versus time for a single flow cycle

the fact that segregation and blocking do not occur for all the aggregate particles, and that the finer aggregate potion can remain uniform suspension during the flow in place of stable SCC. It is important to note that, due to the limits in calculation capacity of computers, tracking of the positions of all the coarse aggregate particles (having typical contents and sizes, ranging from 10% to 30% and 5 mm to 20 mm, respectively) would have been impossible. On the other hand, increasing the number of particles can lead to decreasing the volume of suspending fluid (i.e., paste/mortar matrix in concrete mixture). According to Esmaeilkhanian *et al*. (2014b), decreasing the paste volume (i.e., increasing the solid fraction) can significantly decrease the volumetric dynamic segregation indices. This can be explained by the fact that decreasing the suspending fluid portion results in less interstitial space for solid particles (aggregate particles) to move and segregate. As stated in Esmaeilkhanian *et al*. (2014b), and Philips *et al*. (1992), when particle volume fraction approaches its maximum value (i.e., paste volume reaches its minimum), the plastic viscosity tends towards infinity making any further particle migration virtually impossible. It was shown in Philips *et al*. (1992) that for a flow through a cylinder, increasing particle volume fraction decreased heterogeneities (i.e., dynamic segregation) across the cylinder section. The same phenomenon occurred in the T-Box channel. When the particle volume was increased, the particle distribution along the T-Box remained uniform during the flow, resulting in lower dynamic segregation.

It must also be noted that the effect of five values of suspending fluid plastic viscosity (i.e., 10, 17, 25, 38, and 50 Pa.s) on the flow performance of suspensions is only evaluated for the suspensions having the maximum suspending fluid yield stress value of 75 Pa. On the other hand, the effect of suspending fluid yield stress on flowability and dynamic stability of SCC is only evaluated for the mixtures having the minimum plastic viscosity value of 10 Pa.s.

In total, the first six flow cycles (i.e., t = 12 s) of the tilting motion of the T-Box test was considered in model of the investigated suspensions. As mentioned before, the tilting of the apparatus starts from stationary horizontal state at t = 0 s, and also at the beginning of each flow cycle (i.e., t = 2, 4, 6, 8, and 10 s) by tilting down the channel. Therefore, the initial angular velocity at the beginning of each flow cycle should set to be zero (ω(t = 0, 2, 4, 6, 8, and 10 s) = 0 rad/s). The tilting procedure is ended by a horizontal position at t = 12 s by a tilting up motion (i.e., ω(t = 12 s) = 0 rad/s). On the other hand, since the box edge touches the floor slightly at the end of each first half of the flowing cycles (i.e., t = 1, 3, 5, 7, 9, and 11 s), the corresponding angular velocity of the tilting procedure is assumed to be zero at these flow times. Considering the fact that tilting pattern should be continuous, it also assumed that angular velocity of the apparatus reaches maximum values at first and third quarter flow cycles (i.e., t = 0.5, 1.5, 2.5, 3.5, 4.5, 5.5, 6.5, 7.5, 8.5, 9.5, 10.5, and 11.5 s). On the other hand, the apparatus should be rotated by a maximum angle of α = $\tan^{-1}$(140 mm/500 mm) = 0.273 rad (i.e., 15.642 degree) in every half cycles. Therefore, assuming a sinusoidal function pattern, the angular velocity of modeled T-Box set-ups can be defined as a function of the flow time, according to Eq. (1)

$$\omega(rad/s) = 0.4288\sin(\pi.t) \tag{1}$$

where ω is the angular velocity of the apparatus as function of flow time t, positive and negative values of ω correspond to tilting down and tilting up periods of flow, respectively. A typical example of angular velocity values for a single flow cycle is presented in Fig. 2.

4. Numerical simulation and boundary conditions

In order to simulate flow performance of SCC in the T-Box test apparatus, a CFD software (FLOW3D®) was employed. The basic equations of the conservation of mass for incompressible materials and the Navier-Stokes equations are solved by the Volume of Fluid (VOF) method (Hirt and Nichols 1981). In total, 7 simulations were carried out for a period of flow of 12 s (i.e., 6 flow cycles). Six mesh blocks of 585,104 cubic cells with 5-mm size in the X, Y, and Z directions were created to discretize the geometry, solid elements, and suspension.

As presented in Fig. 3(a-1), the Dirichlet-Neumann boundary conditions were applied based on the geometry of the T-Box set-up; the velocity of the walls of the apparatus was set to zero in Y direction. In the X and Z directions, the velocity of the walls is governed by Eq. (1).

In order to simulate the motion of dynamic boundaries (e.g., T-Box apparatus) and suspended particles in heterogeneous suspensions, a General Moving Object (GMO) technique was employed. A GMO consists in a rigid body subjected to physical motion, which is either dynamically coupled with fluid flow or prescribed. It can move with six degrees of freedom or rotate around a fixed point or a fixed axis. The GMO model allows to have multiple moving objects in one problem, and each moving object can have any independently defined type of motion. GMO components undergo a mixed motion, including coupled translational and/or rotational velocities. Furthermore, a body-fixed reference system (body system) defined for each moving object and the space reference system (space system) are employed. At each time step, the hydraulic force and torque due to pressure, gravitational, and shear stresses are calculated, and equations of motion are solved for the moving objects under the coupled motion due to these forces. Area and volume fractions are recalculated at each time step based on updated object locations and orientations. Source terms are added in the continuity and the VOF transport equations to account for the effect of moving objects to displace the fluid. The tangential velocity of the moving boundaries is introduced into shear stress terms in the momentum equation. An implicit numerical method is employed to calculate in an iterative manner, coupling of fluid flow and GMO motion in each time steps using the force and velocity data from the previous time step (FLOW3D® software user guide).

The GMO model was employed to incorporate and allow rigid collision between spherical particles. The collisions are assumed to be instantaneous and are allowed to occur between moving rigid bodies (i.e., spherical particles), and between rigid bodies and wall boundaries of the computational domain. At each time step, once a collision is detected, a set of impact equations are integrated.

In this study, the collision between particle-particle and particle-wall boundaries of the apparatus are assumed to be perfectly elastic with a coefficient of restitution of 0.8. This value was obtained based on experimental measurements carried out using 20-mm diameter spherical glass beads (having approximately same density as the modelled coarse aggregate) on different surfaces, such as steel and Plexiglas (similar to that one used for T-Box apparatus). These measurements were carried out at the University of Sherbrooke, using high speed camera. Friction at the contact point is also taken into consideration during collision. The friction boundary conditions between particles, fluid, and the walls of the apparatus were considered with a friction coefficient value of 0.4 according to Coulomb's law of friction (Vanhove and Djelal 2013).

The modelled fluids are considered as non-Newtonian Bingham fluids using an elasto-viscoplastic model with implicit time integration. Gravity stresses are calculated using gravitational acceleration value of 9.81 m/s^2. In order to consider particle-particle and particle-wall interactions, a coefficient of restitution of 0.8 was applied for collision physical model. The modelled flow is assumed to be laminar flow type (RILEM 222-SCF). It is worthy to mention that numerical simulations carried out on an i7-2600 CPU 3.40 GHz processor required a total running time between 124 and 592 hours. The running time depend mostly on the plastic viscosity of the suspending fluid. Indeed, the simulation of T-Box flow of higher viscous suspensions took more calculation time than less viscous ones.

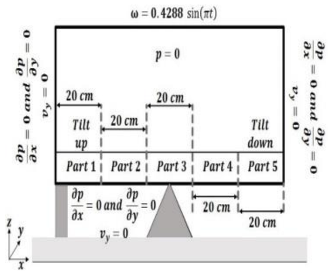

(a-1) Boundary conditions and positions of horizontal sampling parts

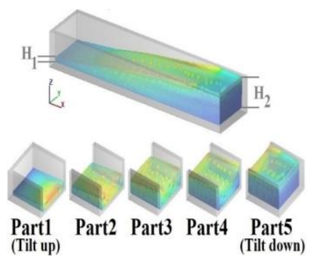

(a-2) Horizontal sampling parts

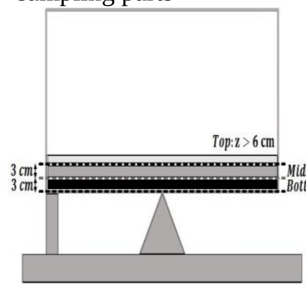

(b-1) Positions of vertical sampling sections

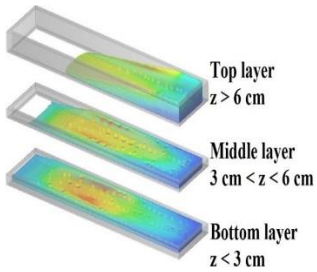

(b-2) Vertical sampling sections

Fig. 3 Boundary conditions and sampling parts

4.1 Sampling methods and anticipated results

In order to evaluate flowability of the modelled suspensions, the results of the simulations are presented in 0.1-s time steps in forms of flow velocity, strain rate, kinetic energy, displacement magnitudes, and flow profiles. Dynamic stability properties of the suspensions in horizontal direction are also calculated by measuring the volumetric particle contents in five 20-cm long sections through the T-Box horizontal channel that are illustrated in Figs. 3(a-1) and 3(a-2). The number and position of the particles, as well as the volume of the fluid in each section are calculated at each flow cycle (i.e., 2-s periods). On the other hand, dynamic stability of the suspensions in the vertical direction is evaluated by comparing the volumetric particle contents in three vertical layers (bottom, middle, and top) at each flow cycle (i.e., 2-s periods). As presented in Figs. 3(b-1) and 3(b-2), the thickness of both the bottom and middle layers is 3 cm, and the remaining (Z > 6 cm) corresponds to the top layer.

5. Results and discussions

5.1 Evaluation of flowability of modelled suspensions in T-Box test set-up

In this section, the flowability of the modelled suspensions with five suspending fluid viscosity values corresponding to 10, 17, 25, 38, and 50 Pa.s, and the same yield stress value of 75 Pa, are evaluated using numerical simulation. Flow profile angles can be calculated at the end

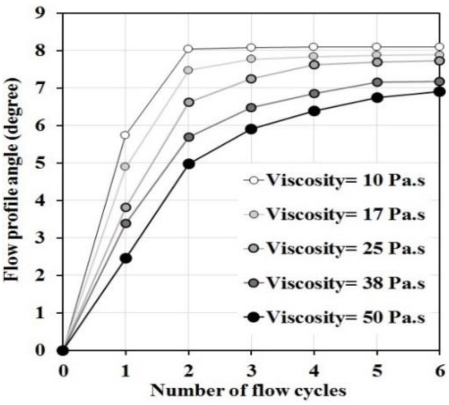

(a) Flow profile angle in each flow cycle versus number of flow cycles

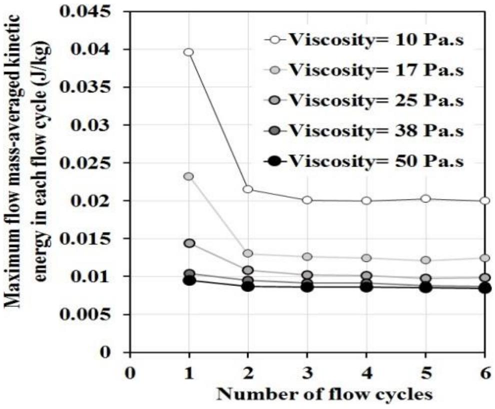

(b) The maximum flow mass-averaged kinetic energy in each flow cycle versus number of flow cycles

Fig. 4(a) Flow profile angle and (b) the maximum flow mass-averaged kinetic energy in each flow cycle versus number of flow cycles

of each flow cycle using Eq. (2).

$$Flow\ profile\ angle\,(\deg) = \tan^{-1}\left(\frac{H_2 - H_1}{L = 1m}\right) \qquad (2)$$

where H_2 and H_1 (Fig. 3(a-2)) are the flow profile depths at the tilt down and tilt up sides of the T-Box at the end of each flow cycle, respectively, and L =1 m is the channel length. The results of flow profile angles at the end of each cycle are presented in Fig. 4(a) for different plastic viscosity values of suspending fluid. As can be observed in Fig. 4(a), for a given viscosity, increasing the number of cycles can result in higher flow profile angle till reach an equilibrium value. Moreover, for a given flow cycle, increasing fluid viscosity results in decreasing the flow profile angle due to the less flowability of higher viscous mixtures. For example, under 2 flow cycles, increasing suspending fluid viscosity from 10 to 50 Pa.s can decrease the flow profile angle from 8.0 to 5.0 degree. Furthermore, it is worthy to mention that increasing the number of flow cycles can lead to decrease the viscosity effect on the angle of flow profile. For example, increasing plastic viscosity of suspending fluid from 10 to 50 Pa.s can decrease the flow profile angle from 5.7 to 2.5 degree (i.e., 56% reduction) and from 8.1 to 6.9 degree (i.e., 15% reduction) under 1 and 6 flow cycles,

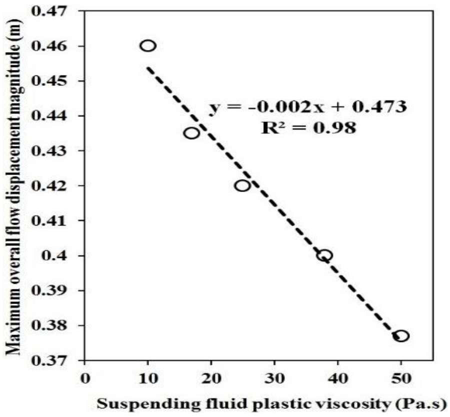

(a) Maximum overall flow displacement, versus suspending fluid plastic viscosity

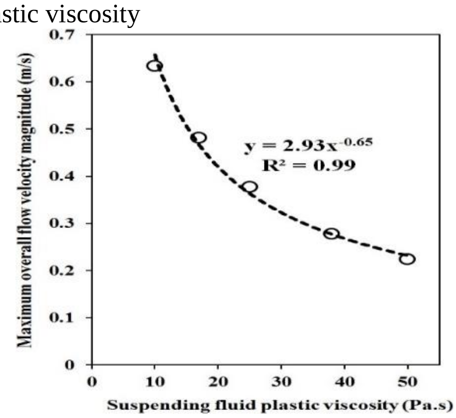

(b) Maximum overall flow velocity versus suspending fluid plastic viscosity

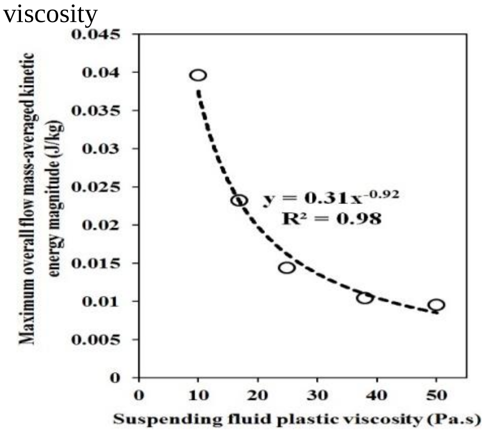

(c) Maximum overall flow mass-averaged kinetic energy versus suspending fluid plastic viscosity

Fig. 5 Flowability properties versus suspending fluid plastic viscosity

respectively. This can be explained by the dissipation of initial flow energy in higher flow displacements obtained by more flowing cycles (Fig. 4(b)). Indeed, in a constant gravitational (i.e., constant density) and elastic (i.e., constant yield stress values) force conditions, when the flow energy becomes less, the effect of viscous forces on free surface flow profile shape of the mixtures also decreases. Accordingly, the maximum values of flow mass-averaged kinetic energy in each flow cycle are presented in Fig. 4(b). As can be observed, flow kinetic energy is mostly dissipated in the second flow cycle due to friction stresses

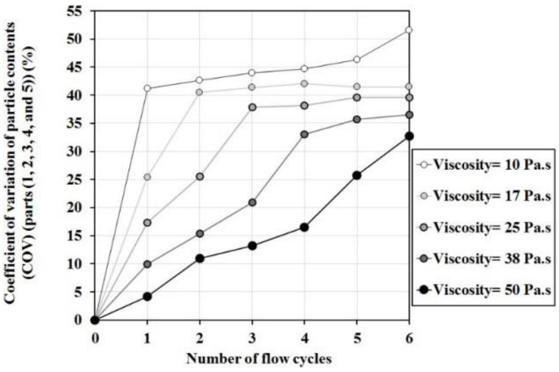

(a) The variation of COV of particle contents in five horizontal sections versus number of flow cycles for different suspending fluid plastic viscosity

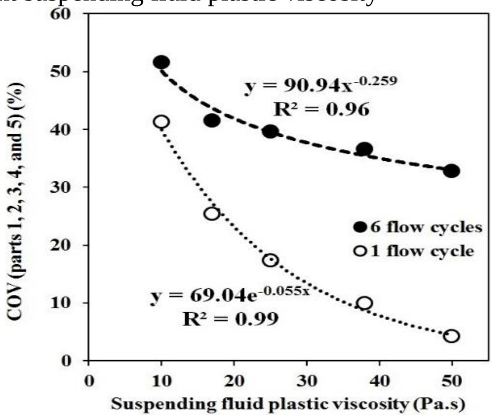

(b) The variation of COV of particle contents in five horizontal sections versus suspending fluid plastic viscosity for 1 and 6 flow cycles

Fig. 6 The variation of COV of particle contents in five horizontal sections versus (a) number of flow cycles for different suspending fluid plastic viscosity, and (b) suspending fluid plastic viscosity for 1 and 6 flow cycles

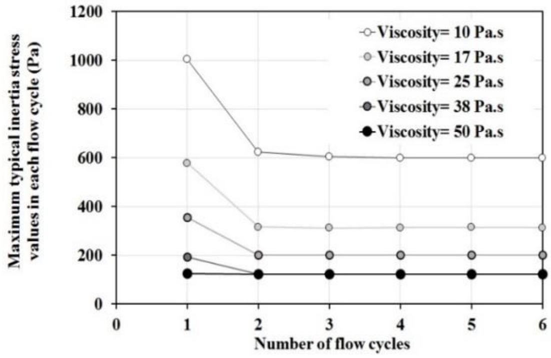

Fig. 7 Maximum typical inertia stress values in each flow cycles for different values of suspending fluid viscosity

and wall effect. After the second cycle, it reaches equilibrium values for each suspension. These effects are shown to be dominant in the case of lower viscosity values. This proves that flow properties of the mixtures with less suspending fluid viscosity are affected mostly by the initial flow energy provided by the first tilting cycle, while for the higher viscous mixtures the number of flow cycles (Eq. (1)) is the most dominant factor. For example, the maximum flow mass-averaged kinetic energy magnitudes in the first flow cycle decrease from 0.0396 to 0.0215 J/kg (i.e., 46% dissipation) and from 0.0095 to 0.0087 J/kg (i.e., 8% dissipation) in the second flow cycle for suspending fluid plastic viscosity values of 10 and 50 Pa.s, respectively.

The results of the maximum overall values of flow displacement, flow velocity, and mass-averaged kinetic energy obtained for the investigated suspensions during the test duration (i.e., t = 0 to 12 s) are presented in Fig. 5(a), 5(b), and 5(c), respectively. Suspensions with lower plastic viscosity of the suspending fluid can exhibit higher flowability. For example, increasing the plastic viscosity of suspending fluid from 10 to 50 Pa.s resulted in decreasing the maximum overall flow displacement, velocity, and mass-averaged kinetic energy magnitudes from 0.460 to 0.377 m (i.e., 18% decrease), 0.634 to 0.224 m/s (i.e., 65% decrease), and 0.0396 to 0.0095 J/kg (i.e., 76% decrease), respectively.

5.2 Evaluation of dynamic stability of suspensions in the horizontal direction

In this section, horizontal dynamic stability of the modeled suspensions with suspending fluid viscosity values of 10, 17, 25, 38, and 50 Pa.s and yield stress value of 75 Pa are evaluated using numerical simulations. Fluid volume and particle contents in five horizontal sampling sections (as presented in Fig. 3(a)) are calculated at the end of each flow cycle. Accordingly, shear-induced dynamic segregation of the mixtures in the horizontal direction can be quantified for each flow cycle using the coefficient of variation (COV) of particle contents in all the five horizontal parts (Eq. (3)).

$$COV\,(\%) = \frac{STANDARD\ DEVIATION\ of\ particle\,contents\ (Parts\,1,2,3,4,and\ 5)}{AVERAGE\ of\ particle\,contents\ \ (Parts\,1,2,3,4,and\ 5)} \qquad (3)$$

As can be observed in Fig. 6(a), for a given suspending fluid viscosity, increasing the number of flow cycles can result in increasing the COV of particle contents in the five horizontal samples, which indicates higher dynamic segregation. This can be due to the increase in flow displacement, which can lead to higher shear-induced heterogeneity in the suspensions. On the other hand, within a given number of flow cycles, the suspensions with higher suspending fluid viscosity show less COV values than those with less suspending fluid viscosity. It is also worthy to mention that increasing the viscosity shows higher effect in the case of less flow cycle numbers due to its effect on the initial flow energy and inertial forces which are provided in the first flow cycle. For example, as can be observed in Fig. 6(b), increasing the plastic viscosity of the suspending fluid from 10 to 50 Pa.s resulted in decreasing the COV from 41% to 4% (i.e., 37% reduction) and from 52% to 33% (i.e., 19% reduction) under 1 and 6 flow cycles, respectively, with very good coefficient of correlation ($R^2 > 0.96$).

It can also be concluded from Fig. 6(b) that increasing the number of flow cycles resulted in less effect on the dynamic segregation of the mixtures with less plastic viscosity value of suspending fluid. For example, increasing the number of flow cycles from 1 to 6 resulted in increasing

COV from 41% to 52% (i.e., 11% increase) and from 4% to 33% (i.e., 29% increase) for suspending fluid viscosity values of 10 and 50 Pa.s, respectively. This can be due to the less drag forces exerted on particles in the case of less viscosity of suspending fluid. Consequently, less viscous mixtures can mostly segregate dynamically in the initial flow cycles (i.e., less flow distance traveled by the suspension) which flow energy and inertia stresses are significantly higher than those values in subsequent flow cycles, and then reaches to an equilibrium value. The results presented in Fig. 4(b) showed that the flow energy is more dissipated after initial flow cycle in the case of less viscous mixtures. Typical maximum values of inertial stress ($I_{max}(i)$) in the flow cycle (i) can also be estimated using Eq. (4).

$$I_{\max}(i) = \rho[V_{\max}(i)]^2 \tag{4}$$

where ρ = 2500 kg/m^3 is the density of the suspension and $V_{max}(i)$ is the maximum flow velocity magnitude in the flow cycle i. It is worthy to mention that within a given flow cycle i, suspensions exhibited their maximum flow velocity ($V_{max}(i)$) in the second quarter of the cycle (i) which refers to the second half of the tilting down steps. Moreover, as the plastic viscosity of suspending fluid increases, the maximum flow velocity for a given number of flow cycle (greater than 1) tends to be obtained mostly at the beginning of the second quarter of that cycle where the angular velocity is at its maximum value. For the less viscous suspensions, this value was obtained mostly at the end of the second quarter of the cycle which corresponds to the end of the tilting down step.

As can be observed in Fig. 7, for the suspending fluid with lower plastic viscosity, inertia stress values decrease significantly after the first flow cycle compared to those with higher viscosity where the inertia stresses remain comparable, regardless of the number of flow cycles. For example, the maximum inertia stress in the first flow cycle decreases from 1005 to 625 Pa (i.e., 38% decrease), and from 125 to 121 Pa (i.e., 3% decrease) in the second flow cycle for suspending fluid plastic viscosity values of 10 and 50 Pa.s, respectively.

Accordingly, higher viscous suspensions reach their maximum dynamic segregation capacity after longer flow cycles (i.e., longer flow distances). For example, as can be observed in Fig. 6(a), 2, 3, and 4 flow cycles are required for the mixtures with suspending fluid viscosity values of 17, 25, and 38 Pa.s, respectively to reach at least 90% of their maximum dynamic segregation capacity which is obtained after 6 flow cycles.

According to Esmaeilkhanian (2011), Esmaeilkhanian *et al*. (2014a) and (2014b), comparison between the properties of two horizontal samples located in tilt up and tilt down sides of the T-Box can also be used as an evaluation index for horizontal dynamic segregation of SCC. Therefore, calculating fluid volume and particle content in two horizontal sampling sections located at the tilt down (Part 5) and tilt up (Part 1) sides of the T-Box channel, the horizontal dynamic segregation index (H.D.S.I.) can be defined for each flow cycle using Eq. (5).

$$H.D.S.I.(\%) = \frac{Particle\ content\ @\ tilt\ down\ side(Part\,5) - Particle\ content\ @\ tilt\ up\ side(Part\,1)}{Initial\ mean\ particle\ content} \times 100\% \tag{5}$$

Similar to the COV, as can be observed in Fig. 8(a), for a given suspending fluid's plastic viscosity, increasing the number of flow cycles can result in increasing the H.D.S.I. values. This can be explained by the fact that under higher flow cycles, the mixture travels more distance in the horizontal direction, which affects the homogeneity of the suspensions. On the other hand, under a given number of flow cycles, higher H.D.S.I. values were obtained for lower suspending fluid plastic viscosity mixtures. This can be due to the higher drag forces exerted on the particles in the case of higher viscosity of suspending fluid which results in maintaining more particles in the suspending fluid and prevents them to segregate. Furthermore, increasing the viscosity results in higher effect in the case of less number of flow cycles due to the effect of viscosity on the initial flow energy and inertial forces, which are provided in the first flow cycle to drive the displacements of the particles. For example, as can be observed in Fig. 8(b), increasing the plastic viscosity of the suspending fluid from 10 to 50 Pa.s can decrease the H.D.S.I. from 91% to 3% (i.e., 88% reduction) and from 101% to 68% (i.e., 33% reduction) after 1 and 6 flow cycles, respectively, with very good coefficient of correlation (R^2 = 0.98).

As can be observed in Fig. 8(b), increasing the number of flow cycles can have a higher effect on the horizontal dynamic stability of the mixtures with higher suspending fluid plastic viscosity. For example, increasing the number of flow cycles from 1 to 6 increased the H.D.S.I. values from 91% to 101% (i.e., 10% increase in horizontal dynamic segregation) and from 3% to 68% (i.e., almost 65% more horizontal dynamic segregation) for suspending fluid viscosity values of 10 and 50 Pa.s, respectively. Indeed, lower viscous mixtures exhibit more dynamic segregation during the first flow cycle (i.e., less flow distance traveled by the suspension), and then they reach an equilibrium value. This can be due to higher initial flow energy (Fig. 4(b)) and inertial stresses (Fig. 7), as well as less drag forces exerted on particles in the initial flow cycles. However, in the case of higher viscous suspensions, more flow cycles (which means higher flow distance) is required to reach the maximum dynamic segregation capacity. As can be observed in Fig. 8(a), the number of flow cycles of 1, 2, 3, and 4 are required for the mixtures with suspending fluid viscosity values of 10, 17, 25, and 38 Pa.s, respectively, to reach almost 90% of their maximum capacity of horizontal dynamic segregation, which is obtained after 6 flow cycles.

5.3 Tracking of particles

In order to validate the results of sections 5.1 and 5.2 the maximum displacements of nine typical particles are calculated for each mixture in a flow time when the mixture reached its maximum flow displacement (i.e., $t_{\text{maximum flow displacement}}$). As presented in Fig. 9, these typical particles are located in three different vertical layers (i.e., top, middle, and bottom) and three different horizontal sections (i.e., tilt down, middle, and tilt up). According to the results presented in Fig. 5(a), for the flow times corresponding to the maximum overall flow displacement

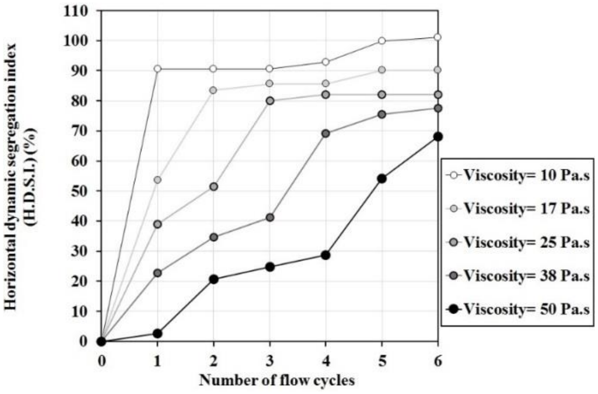

(a) Variation of the horizontal dynamic segregation index (H.D.S.I.) with number of flow cycles and different suspending fluid plastic viscosity
cycles

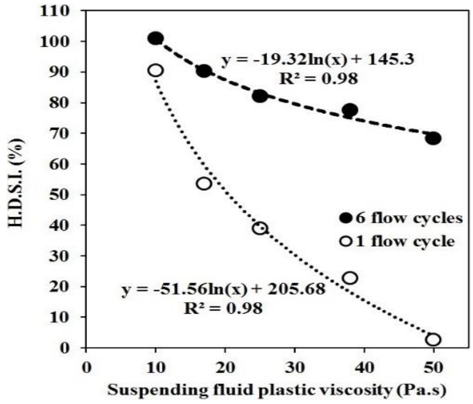

(b) Variation of the horizontal dynamic segregation index (H.D.S.I.) with suspending fluid plastic viscosity for 1 and 6 flow

Fig. 8 Variation of the horizontal dynamic segregation index (H.D.S.I.) with, (a) number of flow cycles and different suspending fluid plastic viscosity, and (b) suspending fluid plastic viscosity for 1 and 6 flow cycles

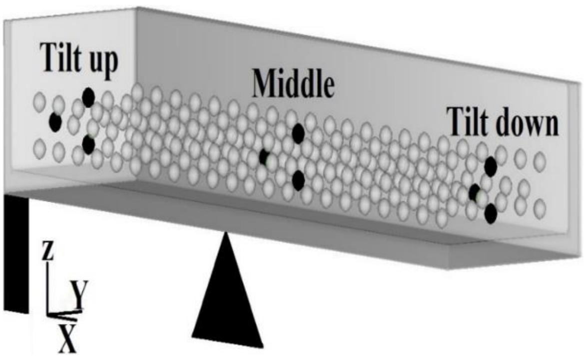

Fig. 9 Initial positions of nine representative 20-mm diameter particles, colored in black

(i.e., $t_{maximum\ flow\ displacement}$ which were obtained as 3.4, 5.4, 9.4, 11.4 and 11.5 s for suspending fluid viscosity of 10, 17, 25, 38, and 50 Pa.s, respectively), displacements of each of nine particles in the X, Y, and Z directions are calculated. The maximum total displacement for each particle can be calculated using Eq. (6), where $Displ_{max}(i)$ is the maximum total displacement of the particle i, and

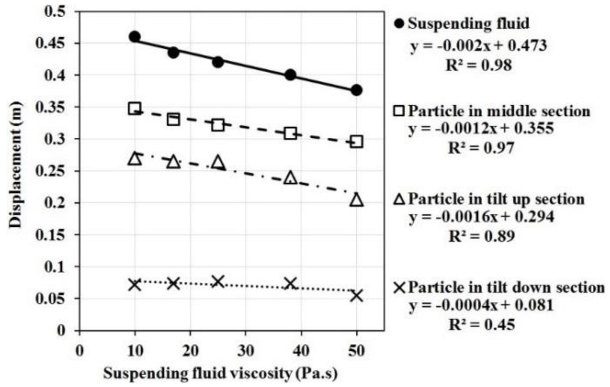

(a) Particles located at top vertical layer and three horizontal sections

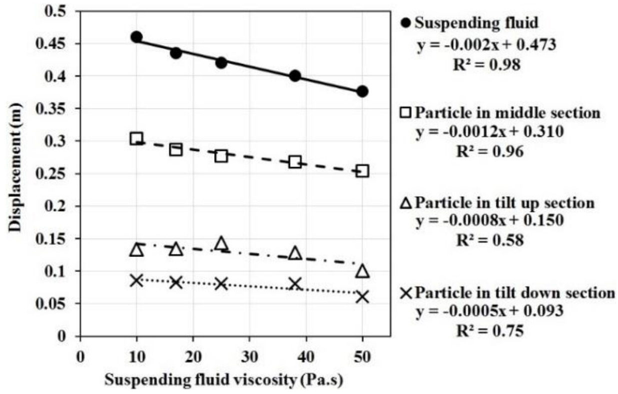

(b) Particles located at middle vertical layer and three horizontal sections

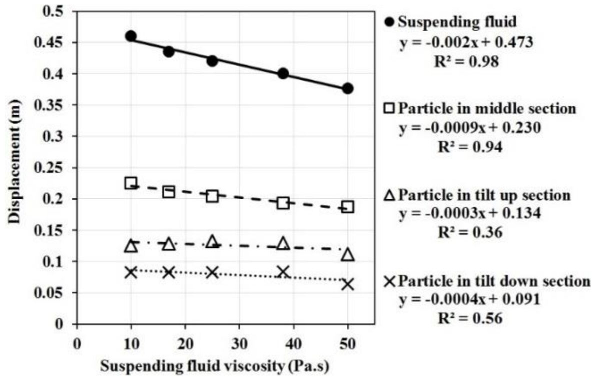

(c) Particles located at bottom vertical layer and three horizontal sections

Fig. 10 The variation of the maximum displacement of suspending fluid and typical particles located in three horizontal sections (tilt up, middle, and tilt down) and three vertical layers (a) top, (b) middle, and (c) bottom with the plastic viscosity of suspending fluid

$Displ_X(i)$, $Displ_Y(i)$, and $Displ_Z(i)$ are the displacements of particle i in X, Y, and Z directions, respectively, for a period of time from 0 to $t_{maximum\ flow\ displacement}$.

The maximum displacement ($Displ_{max}$) values of the particles placed at different initial horizontal and vertical positions are compared to the maximum displacement of the suspending fluid having different plastic viscosities in Figs. 10(a)-(c). According to the results presented in Fig. 10, for suspending fluid viscosity ranging between 10 and 50 Pa.s, all the typical particles placed in different locations exhibited lower displacements than the suspending fluid, which means that the dynamic segregation happened definitely in all locations of the suspension medium. For example, in the case of suspending fluid (viscosity between 10 to 50 Pa.s), the maximum displacement varies between 0.377 and 0.460 m. However, in the case of the typical particles, lower maximum displacement (from 0.055 to 0.348 m) is observed. This can be due to the frictional and drag forces exerted on particles, and also to particle-particle and particle-walls interactions which can lead to reducing the capacity of suspending fluid to transport the particles.

However, in the case of particles located in the middle horizontal section, more displacement is observed compared to those located in tilt up and tilt down sections. This can be due to lower interactions with side walls of the T-Box. For example, particles located in the middle, tilt up, and tilt down horizontal sections exhibit displacements from 0.187 to 0.348 m, 0.101 to 0.270 m, and 0.055 to 0.086 m, respectively, regardless of their vertical locations.

$$Displ_{\max}(i) = \sqrt{Displ_X(i)^2 + Displ_Y(i)^2 + Displ_Z(i)^2} \quad (6)$$

Therefore, it can also be concluded that the particles placed initially in the tilt down section exhibit the minimum displacement values. This can be explained by the accumulation of particles and formation of an internal structure in the tilt down section, which is called lattice effect (Körner *et al*. 2005, Man and van Mier 2011, Eliáš and Stang 2012). This can resist against more particle displacement in the tilt down section.

As can be observed in Fig. 10, the viscosity of suspending fluid did not show a significant effect on displacement of the particles in the tilt down section. For example, increasing the viscosity from 10 to 50 Pa.s resulted in decreasing in the displacement of particles located in the tilt down side from 0.072 to 0.055 m (i.e., 0.017 m decrease), 0.086 to 0.061 m (i.e., 0.025 m decrease), and 0.083 to 0.064 m (i.e., 0.019 m decrease) for top, middle, and bottom initial vertical positions, respectively. These decrements are negligible comparing to particle diameters (i.e., 0.02 m). This is due to the lattice effect and interaction between particles and side walls of the T-Box which are more dominant than the effect of viscosity of suspending fluid.

On the other hand, particles located in the top layer show larger ranges of displacement than those placed in the middle and bottom layers due to lower distance from the flow surface, and accordingly, less friction and interaction with surrounding fluid and solid walls. For example, regardless of the initial horizontal positions, typical particles located initially in the top, middle, and bottom layers show displacements from 0.055 to 0.348 m, 0.061 to 0.304 m, and 0.064 to 0.226 m, respectively.

As can be observed, increasing the viscosity of suspending fluid resulted in decreasing displacement of particles that are mostly located in the middle and tilt up horizontal sections of the top layer (i.e., Fig. 10(a)). For example, increasing the viscosity from 10 to 50 Pa.s decreases displacement of particles located in the tilt up and middle sections of the top layer from 0.270 to 0.205 m (i.e., 0.065 m decrease) and 0.348 to 0.296 m (i.e., 0.052 m decrease), respectively.

However, as can be observed in Fig. 10, the viscosity of suspending fluid has no significant effect on displacement of particles located initially in bottom layer, which showed the minimum displacements compared to other vertical layers, especially for those placed in tilt up and tilt down horizontal sections. For example, increasing viscosity of the suspending fluid from 10 to 50 Pa.s decreases displacement of particles which are located initially in the tilt up and tilt down sections of the bottom layer from 0.125 to 0.112 m (i.e., 0.013 m decrease), and 0.083 to 0.064 m (i.e., 0.019 m), respectively. These decrements are lower than diameters of the particles (i.e., 0.02 m) and, therefore, can be considered negligible. This can be due to the dominant effect of friction, particle-particle, and particle-walls interactions on flow performance of the suspension at two bottom corners of the horizontal channel, due to lower distance to the base-plate and side walls of the apparatus. It can also be due to the lattice effect of the internal structure of the particles settled down in the bottom layer. Migration of particles towards the bottom layer is called vertical dynamic segregation and will be discussed in the next section.

5.4 Evaluation of dynamic stability of the suspensions in the vertical direction

As observed in the previous section, the migration of particles towards the bottom layer (i.e., vertical dynamic segregation) has significant effect on displacement of particles through the suspending fluid. In order to determine in which flow depth there is more deformation that may indicate a risk of dynamic segregation in the vertical direction, the ratio of the maximum flow velocity to the maximum strain rate is examined for all the investigated mixtures and for the whole flow period (i.e., t = 0 to 12 s) (Fig. 11). The critical flow thickness of segregation ($h_{critical}$) may be approximated as follows (Eq. (7))

$$h_{critical} \cong \frac{V_{\max}}{\dot{\gamma}_{\max}} \quad (7)$$

where V_{max} is the maximum velocity and $\dot{\gamma}_{max}$ is the corresponding maximum shear strain rate magnitude for each time step. As can be observed in Fig. 11, the critical flow thickness of segregation values ($h_{critical}$) are ranging between 0.0066 and 0.0315 m. This means that particles settle down mostly in a vertical layer located in approximately 0.03-m thickness from the bottom of the channel. It proves that the dimensions for the vertical sampling layers, presented in Fig. 2(b), were properly selected. Therefore, vertical dynamic segregation of the investigated mixtures are evaluated in three vertical layers of top, middle, and bottom, where the thickness of both bottom and middle layers is 3 cm and the remaining (Z > 6 cm) corresponds to the top layer. Moreover, as can be observed in Fig. 11, the darker data points corresponding to the higher suspending fluid viscosity are more collected close the minimum estimated boundary (i.e., $h_{critical}$ = 0.0066 m). On the other hand, data points representing the lower viscosity (brighter data points) tend to the maximum

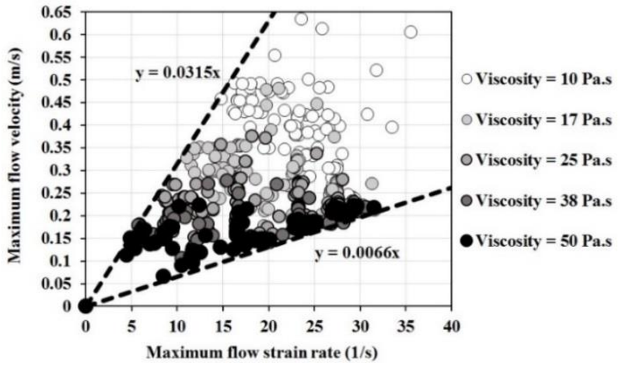

Fig. 11 Maximum flow velocity versus maximum flow strain rate

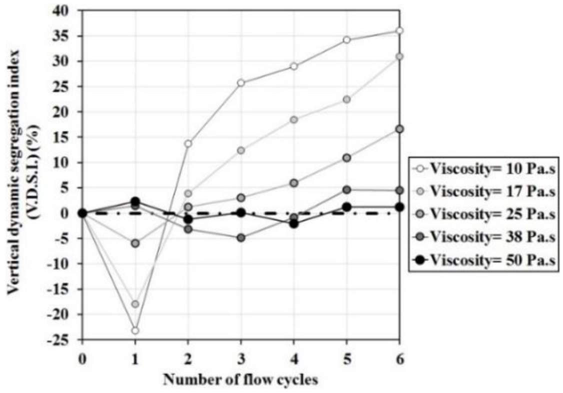

Fig. 12 Vertical dynamic segregation index (V.D.S.I.) versus the number of flow cycles

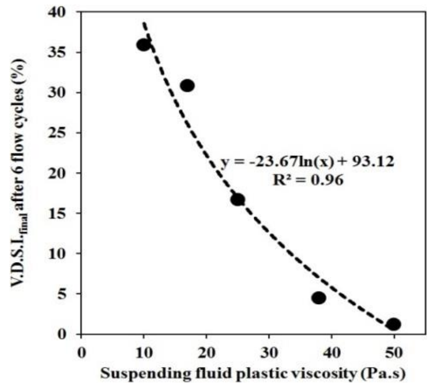

Fig. 13 Vertical dynamic segregation index after 6 flow cycles (V.D.S.I.$_{final}$) versus plastic viscosity of suspending fluid

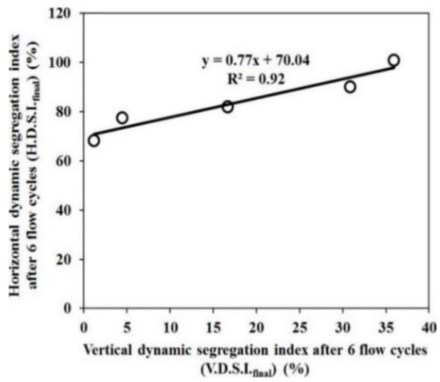

Fig. 14 H.D.S.I.$_{final}$ versus V.D.S.I.$_{final}$

boundary of $h_{critical}$ = 0.0315 m. Therefore, higher vertical dynamic segregation is expected for suspensions with lower suspending fluid viscosity values.

The vertical dynamic segregation index in flow cycle i (i.e., V.D.S.I. (i)) can be defined as the ratio of the difference between the particle content at the top and bottom layers obtained in flow cycle i to the initial particle content as follows

$$V.D.S.I.(i)(\%) = \frac{Particle\ content\ @\ bottom\ layer\ (i) - Particle\ content\ @\ top\ layer\ (i)}{Initial\ mean\ particle\ content} \times 100\% \tag{8}$$

The V.D.S.I. values obtained for different flow cycles are presented in Fig. 12 for the investigated mixtures. As can be observed, in the first flow cycle, the mixtures with lower suspending fluid viscosity of 10, 17, and 25 Pa.s exhibited negative V.D.S.I. values of -23%, -18%, and -6%, respectively, which means having more particle content in the top layer than the bottom one (i.e., inverse vertical dynamic segregation). This can be due to the fact that in the case of lower viscosity, the effect of inertia and initial flow energy on flow displacements of the particles are more dominant than drag capacity of the suspending fluid. On the other hand, as was observed earlier in Fig. 4(a), considering the higher flow profile angles of less viscous suspensions in the first flow cycle, particles tend to move more toward the top layer rather than the bottom one. However, after dissipation of the initial flow energy (Figs. 4(b) and 7), increasing the number of flow cycles resulted in increasing vertical dynamic segregation indices for lower viscosity values. For example, increasing the number of flow cycles from 2 to 6 increases the V.D.S.I. values by 22%, 27%, and 16% for viscosity values of 10, 17, and 25 Pa.s, respectively.

However, in the case of suspending fluid having higher relatively viscosity values (i.e., 38 and 50 Pa.s), the mixtures did not show a significant vertical dynamic segregation after several flow cycles. For example, the V.D.S.I. values between -5% to +5% and -2% to +2% were obtained for suspending fluid viscosity values of 38 and 50 Pa.s, respectively and, therefore, these mixtures can be considered as dynamically stable mixtures in vertical direction.

As presented in Fig. 13, the final values of vertical dynamic segregation index after 6 flow cycles (i.e., V.D.S.I.$_{final}$) are correlated to the plastic viscosity of the suspending fluids. As can be observed, increasing the plastic viscosity of the suspending fluid from 10 to 50 Pa.s can result in decreasing the vertical dynamic segregation indices after 6 flow cycles (i.e., V.D.S.I.$_{final}$) by 35%, with a high R^2 of 0.96. This can be due to increasing effect of suspending fluid viscosity on drag forces exerted on the particles, which can lead to decrease the particle settlements towards the bottom layer.

5.5 Comparison between horizontal and dynamic segregation indices (H.D.S.I. vs V.D.S.I.)

In order to assess the ability of T-Box test to evaluate dynamic stability of SCC in different directions, the horizontal and vertical dynamic segregation indices after 6 flow cycles are compared for all the investigated suspensions.

As can be observed in Fig. 14, under 6 flow cycles of T-Box test, the investigated mixtures showed higher dynamic segregation in the horizontal direction (68% < H.D.S.I.$_{\text{final}}$ < 101%) than the vertical one (1% < V.D.S.I.$_{\text{final}}$ < 36%). Therefore, this set-up can be recommended for horizontal applications, such as these of casting long wall, beam, and slab elements, where the horizontal displacement is higher than the vertical one.

5.6 Effect of yield stress of suspending fluid on flow performance of suspensions in T-Box set-up

According to the results of the previous sections, the maximum flowability and dynamic segregation in both horizontal and vertical directions were obtained for the suspending fluid with the lowest viscosity (10 Pa.s) investigated in this study. In this section, the effect of three different yield stress values of suspending fluid (i.e., 14, 45, and 75 Pa) on flow performance of suspensions under 6 flow cycles (i.e., 12-s flow time) is studied only for the mixtures with suspending fluid having a plastic viscosity of 10 Pa.s. The results of these simulations are summarized in Table 1.

As can be observed in Table 1, for a given viscosity of the suspending fluid (10 Pa.s), increasing the yield stress of the suspending fluid can decrease both flowability and dynamic segregation of suspensions in both horizontal and vertical directions. For example, in the case of flowability properties, increasing the yield stress of the suspending fluid from 14 to 75 Pa can lead to 17%, 20%, 27%, and 36% decrease in the maximum magnitudes of flow displacement, velocity, mass-averaged kinetic energy, and strain rate of the suspensions, respectively. However, by comparing to those flowability results presented in section 5.1, it can be concluded that the yield stress of suspending fluid showed less effect on flowability of suspension in T-Box test set-up than plastic viscosity. Increasing the suspending fluid plastic viscosity can decrease flow velocity and mass-averaged kinetic energy magnitudes by 65% and 76%, respectively, which are almost three times higher than those obtained due to the increase the yield stress (i.e., 20% and 27%).

On the other hand, according to the results of the numerical simulations presented in Table 1, increasing the yield stress of suspending fluid from 14 to 75 Pa is showed to reduce the maximum COV, H.D.S.I., and V.D.S.I. values after 6 flow cycles by 15%, 12%, and 10% respectively. However, comparing to the results presented in the sections 5.2 and 5.4, it can be concluded that the plastic viscosity of suspending fluid has more significant effect on dynamic segregation of the investigated suspensions in T-Box test than the yield stress. Indeed, increasing the suspending fluid plastic viscosity resulted in higher reduction in the maximum values of COV, H.D.S.I., and V.D.S.I. by 19%, 33%, and 35% values, respectively, compared to those obtained by the increase in yield stress (i.e., 15%, 12%, and 10% reduction, respectively). This can be due to the fact

Table 1 Flowability properties and dynamic segregation for different yield stress values of the suspending fluid with constant viscosity of 10 Pa.s (μ_p is the plastic viscosity and τ_0 is the yield stress of the suspending fluid)

Rheological properties of suspending fluid		Flowability properties				Dynamic segregation		
						Horizontal direction		Vertical direction
μ_p (Pa.s)	τ_0 (Pa)	Maximum flow displacement (m)	Maximum flow velocity (m/s)	Maximum flow mass-averaged kinetic energy (J/kg)	Maximum flow strain rate (1/s)	Maximum COV (%) (Eq. (3))	Maximum H.D.S.I. (%) (Eq. (5))	Maximum V.D.S.I. (%) (Eq. (8))
	14	0.554	0.794	0.0546	55.6	67	113	46
10	45	0.482	0.708	0.0462	42.6	59	108	45
	75	0.460	0.634	0.0396	35.6	52	101	36

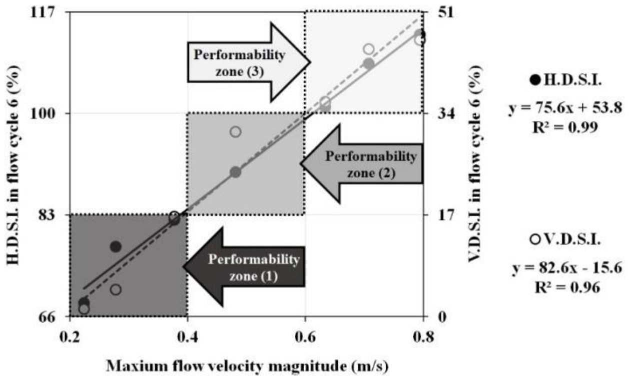

(a) H.D.S.I. and V.D.S.I. values after 6 flow cycles versus maximum flow velocity

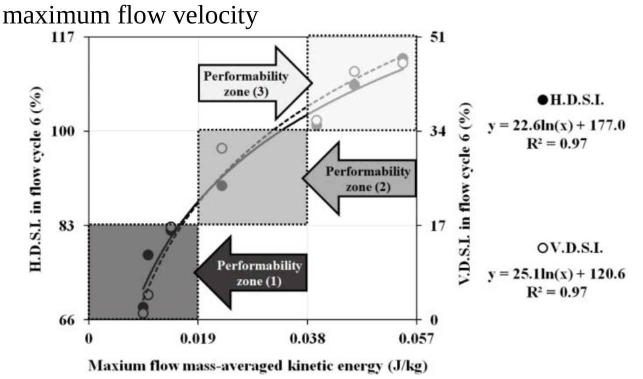

(b) H.D.S.I. and V.D.S.I. values after 6 flow cycles versus maximum flow mass-averaged kinetic energy

Fig. 15 Classification of modelled suspensions based on "performability" properties: The maximum dynamic stability indices in both horizontal and vertical directions versus the maximum magnitudes of (a) flow velocity and (b) mass-averaged kinetic energy

that flow characteristics of suspensions were recorded when the flowing mixture is under shear stress, which has already overcame the yield stress. Therefore, these properties are more influenced by the plastic viscosity than yield stress.

5.7 Proposed approach to evaluate "performability" of suspensions

"Non-restricted dynamic performability" can be defined as the ability of SCC to flow under its own weight through every corner of the formwork while maintaining homogeneity (i.e., uniform suspension of coarse particles), regardless of the presence of reinforcement bars. Therefore, performability is a trade-off between flowability and dynamic stability of SCC (Khayat 1999). Accordingly, the maximum values of simulated dynamic segregation index in both horizontal and vertical directions after 6 flow cycles in T-Box test are correlated to the maximum flow velocity and mass-averaged kinetic energy magnitudes obtained in the T-Box test (Fig. 15).

As can be observed in Fig. 15, the investigated suspensions exhibited the maximum values of flow velocity, mass-averaged kinetic energy, H.D.S.I., and V.D.S.I. indices ranging from 0.224 to 0.794 m/s, 0.0095 to 0.0546 J/kg, 68% to 113%, and 1% to 46%, respectively. It is worthy to mention that the maximum dynamic segregation indices (H.D.S.I. and V.D.S.I. after 6 flow cycles) are well correlated to flowability measurements (i.e., maximum flow velocity and kinetic energy) having correlation coefficients (R^2) higher than 0.96. As can also be observed, increasing flowability of the suspension can reduce its dynamic stability. For example, increasing the maximum flow velocity and mass-averaged kinetic energy obtained for the investigated mixtures by 254% and 475%, respectively, resulted in increasing the maximum values of horizontal and vertical dynamic segregation indices (obtained after 6 flow cycles), by almost 45% (i.e., increasing H.D.S.I. and V.D.S.I. indices from 68% and 1% to 113% and 46%, respectively).

According to the results presented in Fig. 15, three different zones of performability can be defined. This classification corresponds to the three H.D.S.I. ranges of 66%-83%, 83%-100%, and 100%-117% and V.D.S.I. ranges of 0%-17%, 17%-34%, and 34%-51%. These values are obtained after 6 flow cycles. The trade-off between flowability and dynamic stability properties can be observed in these three performability zones, as follows:

Performability zone 1: This zone corresponds to the suspensions which showed a low level of flowability (i.e., the ranges of maximum velocity and mass-averaged kinetic energy of 0.2 to 0.4 m/s, and 0 to 0.019 J/kg, respectively), but a high level of dynamic stability (maximum H.D.S.I. and V.D.S.I. indices in the ranges of 66% to 83% and 0% to 17%, respectively).

Performability zone 2: This zone consists of the suspensions which showed a medium level of flowability (i.e., maximum velocity and mass-averaged kinetic energy of 0.4 to 0.6 m/s, and 0.019 to 0.038 J/kg, respectively). In this zone, the mixtures also exhibited a medium level of dynamic stability (maximum H.D.S.I. and V.D.S.I. indices in the ranges of 83% to 100% and 17% to 34%, respectively).

Performability zone 3: This zone includes the suspensions which showed a high level of flowability (i.e., maximum velocity and mass-averaged kinetic energy of 0.6 to 0.8 m/s, and 0.038 to 0.057 J/kg, respectively), but a low level of dynamic stability having the maximum H.D.S.I. and V.D.S.I. indices in the ranges of 100% to 117% and 34% to 51%, respectively.

According to the results presented in Fig. 15, a general classification based on the relationship between performability and rheological parameters of the suspending fluid can be established, as follows:

Zone 1: This zone includes mixtures with suspending fluids with high yield stress values (75 Pa) and medium to high plastic viscosity values (25 to 50 Pa.s).

Zone 2: This zone includes mixtures made of suspending fluids having high yield stress values (75 Pa) and low plastic viscosity values (17 Pa.s).

Zone 3: This zone consists of the suspensions containing the suspending fluid with low to high yield stress values (14 to 75 Pa) and very low plastic viscosity values (10 Pa.s).

6. Conclusions

In this paper, a CFD software was used to evaluate the effect of rheological properties on non-restricted flowability and dynamic stability of SCC using a T-Box test set-up. The numerical results are in qualitative agreement with those obtained experimentally by Esmaeilkhanian *et al*. (Esmaeilkhanian 2011, Esmaeilkhanian *et al*. 2014a and 2014b). Various suspending fluids, representing the stable and homogeneous portion of concrete, with plastic viscosity, yield stress, and density values of 10 to 50 Pa.s, 14 to 75 Pa, and 2500 kg/m^3, respectively, were investigated. The modelled suspensions consisted of 178 spherical particles in total, with 20-mm diameter (i.e., 4.7% volumetric content) and the same density as the suspending fluid has. Dynamic stability of the suspensions in the T-Box test were evaluated using calculated particle contents of five different horizontal sections and three different vertical sampling layers for different flow cycles. The main concluding remarks are as follows:

• Increasing plastic viscosity of the suspending fluid from 10 to 50 Pa.s can lead to a decrease of the maximum flow displacement, velocity, mass-averaged kinetic energy, and horizontal and vertical dynamic segregation indices by 18%, 65%, 76%, 33%, and 35%, respectively. These reductions are higher than those obtained by increasing the yield stress of the suspending fluid from 14 to 75 Pa (i.e., 17%, 20%, 27%, 12%, and 10%, respectively).

• Increasing the number of flow cycles has more dominant effect on flowability and horizontal dynamic segregation of SCC in the T-Box test set-up for more viscous suspending fluids, while, flow properties of the mixtures with less suspending fluid viscosity are mostly affected by the initial flow energy provided by the first tilting cycle. Indeed, the mixtures with lower viscosity of suspending fluid mostly segregate dynamically in the initial flow cycles (i.e., less flow distance traveled by the suspension), while for higher viscous suspensions, more flow cycles are required to reach the maximum dynamic segregation capacity.

• Simulations revealed that the particles located in the middle horizontal section and top vertical layer exhibited the maximum displacements. On the other hand, the minimum ranges of displacements were obtained for the particles located in the tilt down horizontal section and bottom vertical layer. No significant effect of the plastic viscosity on the displacements of these particles can be observed. This can be due to the more dominant effect of frictional stresses and lattice effect of segregated particles in these sections compared to the plastic viscosity of suspending fluid.

• Higher dynamic segregation in horizontal direction (H.D.S.I. values ranging from 68% to 101%) was obtained compared to vertical direction (V.D.S.I. values ranging between 1% and 36%) in the T-Box test set-up.

• A new definition and approach were proposed to classify the suspensions based on "non-restricted dynamic performability". This is based on a trade-off between flowability and dynamic stability in both the vertical and horizontal directions. Accordingly, the investigated mixtures were classified in three zones of performability: Zone 1 corresponds to low flowable, but high dynamically stable mixtures. Zone 2 corresponds to medium flowable and medium dynamically stable mixtures. On the other hand, zone 3 consists of high flowable, but low dynamically stable mixtures. This classification can be used as a practical tool to choose a proper combination of rheological parameters of the suspending fluid (mortar or stable and homogeneous portion of concrete mixture) to achieve the required flowability and dynamic stability demands in casting process. The rheology of suspending fluid can be modified by decreasing the water to powder material ratio and/or adding higher content of viscosity modifying agent.

Acknowledgments

The authors wish to thank the financial support of the National Science and Engineering Research Council of Canada (NSERC) and the 16 industrial partners participating in the NSERC Chair on High Performance Flowable Concrete with Adapted Rheology held by Professor Khayat of the Université de Sherbrooke in 2008-2013.

References

ACI Committee 237 (2007), *Self-Consolidating Concrete*, American Concrete Institute, Farmington Hills, U.S.A.

Assaad, J., Khayat, K.H. and Daczko, J. (2004), "Evaluation of static stability of self-consolidating concrete", *ACI Mater. J.*, **101**(3), 207-215.

ASTM C1712-14 (2014), *Standard Test Method for Rapid Assessment of Static Segregation Resistance of Self-Consolidating Concrete Using Penetration Test*, West Conshohocken, Pennsylvania, U.S.A.

Eliáš, J. and Stang, H. (2012), "Lattice modeling of aggregate interlocking in concrete", *J. Fract.*, **175**(1), 1-11.

Esmaeilkhanian, B. (2011), "Dynamic stability of self-consolidating concrete: Development of test methods and influencing parameters", M.S. Dissertation, Université de Sherbrooke, Sherbrooke, Canada.

Esmaeilkhanian, B., Feys, D., Khayat, K.H. and Yahia, A. (2014a), "New test method to evaluate dynamic stability of self-consolidating concrete", *ACI Mater. J.*, **111**(3), 299-308.

Esmaeilkhanian, B., Khayat, K.H., Yahia, A. and Feys, D. (2014b), "Effects of mix design parameters and rheological properties on dynamic stability of self-consolidating concrete", *Cement Concrete Compos.*, **54**, 21-28.

FLOW3D® Software User Guide, Flow Science Inc (2016), https://www.flow3d.com.

Gunes, D.Z., Scirocco, R., Mewis, J. and Vermant, J. (2008), "Flow-induced orientation of non-spherical particles: Effect of aspect ratio and medium rheology", *J. Non-Newton. Flu. Mech.*, **155**(1-2), 39-50.

Hirt, C.W. and Nichols, B.D. (1981), "Volume of fluid (VOF) method for the dynamics of free boundaries", *J. Comput. Phys.*, **39**(1), 201-225.

Khayat, K.H. (1999), "Workability, testing, and performance of self-consolidating concrete", *ACI Mater. J.*, **96**(3), 346-353.

Khayat, K.H. and Mitchell, D. (2009), *Self-Consolidating Concrete for Precast, Prestressed Concrete Bridge Elements*, National Cooperative Highway Research Program (NCHRP), Washington, D.C., U.S.A.

Khayat, K.H., Assaad, J. and Daczko, J. (2004), "Comparison of field-oriented test methods to assess dynamic stability of self-consolidating concrete", *ACI Mater. J.*, **101**(2), 168-176.

Körner, C., Thies, M., Hofmann, T., Thürey, N. and Rüde, U. (2005), "Lattice Boltzman model for free surface flow for modeling foaming", *J. Stat. Phys.*, **121**(1), 179-196.

Leighton, D. and Arcrivos, A. (1987), "The shear-induced migration of particles in concentrated suspensions", *J. Flu. Mech.*, **181**, 415-439.

Liao, C.C., Lan, H.W. and Hsiau, S.S. (2016), "Density-induced granular segregation in a slurry rotating drum", *J. Multiph. Flow*, **84**, 1-8.

Man, H.K. and Van Mier, J.G.M. (2011), "Damage distribution and size effect in numerical concrete from lattice analyses", *Cement Concrete Compos.*, **33**(9), 867-880.

Philips, R.J., Armstrong, R.C., Brown, R.A., Graham, A.L. and Abbott, J.R. (1992), "A constitutive equation for concentrated suspensions that accounts for shear-induced particle migration", *Phys. Flu. A*, **4**(1), 30-40.

RILEM State of the Art Report, Technical committee 222-SCF (2014), *Simulation of Fresh Concrete Flow*, Springer.

Roussel, N., Geiker, M.R., Dufour, F., Thrane, L.N. and Szabo, P. (2007), "Computational modeling of concrete flow: General overview", *Cement Concrete Res.*, **37**(9), 1298-1307.

Roussel, N., Gram, A., Cremonesi, M., Ferrara, L., Krenzer, K., Mechtcherine, V., Shyshko, S., Skocec, J., Spangenberg, J., Svec, O., Thrane, L.N. and Vasilic, K. (2016), "Numerical simulations of concrete flow: A benchmark comparison", *Cement Concrete Res.*, **79**, 265-271.

Shen, L., Jovein, H.B. and Li, M. (2014), "Measuring static stability and robustness of self-consolidating concrete using modified segregation probe", *Constr. Build. Mater.*, **70**, 210-216.

Shen, L., Jovein, H.B. and Wang, Q. (2015a), "Correlating aggregate properties and concrete rheology to dynamic segregation of self-consolidating concrete", *J. Mater. Civil Eng.*, **28**(1), 040150671-040150679.

Shen, L., Jovein, H.B., Sun, Z., Wang, Q. and Li, W. (2015b), "Testing dynamic segregation of self-consolidating concrete", *Constr. Build. Mater.*, **75**, 465-471.

Shen, L., Struble, L. and Lange, D.A. (2009), "Modeling dynamic segregation of self-consolidating concrete", *ACI Mater. J.*, **106**(4), 375-380.

Sonebi, M., Rooney, M., Bartos, P.J.M., (2007), "Test method to evaluate dynamic segregation resistance of fresh self-compacting concrete using the settlement column test", *Proceedings of the 5th International RILEM Symposium on Self-Compacting Concrete*, Ghent, Belgium, September.

Spangenberg, J., Roussel, N., Hattel, J.H., Sarmiento, E.V., Zirgulis, G. and Geiker, M.R. (2012a), "Patterns of gravity induced aggregate migration during casting of fluid concretes", *Cement Concrete Res.*, **42**(12), 1571-1578.

Spangenberg, J., Roussel, N., Hattel, J.H., Stang, H., Skocek, J. and Geiker, M.R. (2012b), "Flow induced particle migration in fresh concrete: Theoretical frame, numerical simulations and experimental results on model fluids", *Cement Concrete Res.*, **42**(4), 633-641.

Thrane, L.N. (2007), "Form filling with self-compacting concrete", Ph.D. Dissertation, Danish technological Institute, Kongens Lyngby.

Turgut, P., Turk, K. and Bakirci, H. (2012), "Segregation control of SCC with a modified L-box apparatus", *Mag. Concrete Res.*, **64**(8), 707-716.

Vanhove, Y. and Djelal, C. (2013), "Friction mechanisms of fresh concrete under pressure", *J. Civil Eng. Technol.*, **4**(6), 67-81.

Yammine, J., Chaouche, M., Guerinet, M., Moranville, M. and Roussel, N. (2008), "From ordinary rheology concrete to self compacting concrete: A transition between frictional and hydrodynamic interactions", *Cement Concrete Res.*, **38**(7), 890-896.

Zhaosheng, Y., Xueming, S. and Tanner, R. (2007), "Dynamic simulation of shear-induced particle migration in a two-dimensional circular couette device", *Chin. J. Chem. Eng.*, **15**(3), 333-338.

CC